Chemical Engineering Journal 475 (2023) 146162

Contents lists available at ScienceDirect

Chemical Engineering Journal

journal homepage: www.elsevier.com/locate/cej

Dual crosslinking of low-methoxyl pectin by calcium and europium for the simultaneous removal of pharmaceuticals and divalent heavy metals

Javier Martínez-Sabando [a,b], Francesco Coin [a,b], Juan Carlos Raposo [c], Aitor Larrañaga [c], Jorge H. Melillo [d], Silvina Cerveny [a,d,*]

[a] Centro de Física de Materiales (CSIC, UPV/EHU)-Materials Physics Center (MPC), Paseo Manuel de Lardizabal 5, San Sebastián 20018, Spain
[b] Departamento Polímeros y Materiales Avanzados: Física, Química y Tecnología, University of the Basque Country (UPV/EHU), P. Manuel Lardizábal 3, San Sebastián 20018, Spain
[c] SGIker, General Research Services, University of the Basque Country (UPV/EHU), (48940), Spain
[d] Donostia International Physics Center (DIPC), San Sebastián 20018, Spain

ARTICLE INFO

Keywords:
Pectin
Adsorption kinetics
Water treatment
Crosslinking
Emerging contaminants

ABSTRACT

The contamination of water resources by heavy metals and pharmaceuticals is a significant threat to human health and the environment. Pectin is a promising material for removing heavy metals from water. However, its removal efficacy for other types of pollutants is limited. In this study, we developed a novel approach to enhance the remediation capacity of pectin (with a low degree of methylation) by crosslinking it with different agents: calcium, europium, and their combination. We performed scanning electron microscopy, infrared spectroscopy, and X-ray diffraction experiments to understand the molecular structure of pectin after gelation with the three agents. Our results showed that calcium, europium, and their combination all induce the gelation of pectin. However, the reticulated pectin structures exhibited significant structural differences depending on the type of crosslinking agent used, which affected the adsorption capacity. Specifically, calcium cations partially formed a crystalline "egg-box" structure, whereas europium cations produced a more homogeneous network without crystalline regions. The dual-crosslinking system comprising calcium and europium cations resulted in an intermediate network with both crystalline and amorphous regions. Our findings suggest that dual-cross-linked pectin is a highly effective adsorbent for the simultaneous removal of both heavy metals and pharmaceutical products. This novel approach of crosslinking pectin with multiple agents has the potential to significantly enhance its remediation capacity, offering a promising solution for the simultaneous removal of multiple pollutants from water.

1. Introduction

Chemical contamination of water bodies and water shortages due to overexploitation have increased the need for effective water treatment and decontamination processes. However, current methods of removing pathogens, organic impurities, and salts from water require large amounts of energy [1,2]. Moreover, new contaminants appear in rivers because of the generation of new chemicals at a high rate [3]. Hence, it is essential to develop affordable and efficient water treatment methods to address the growing demand for clean water while conserving energy.

Conventional water treatment processes are often energy intensive, making it necessary to explore new and innovative technologies. Adsorption is a promising technique for decontaminating water and has been used for a long time. Compared with other methods, it is relatively inexpensive and can be implemented in water treatment plants or domestic treatments without excessive energy consumption. Adsorbents can be environmentally friendly if the materials used in their fabrication are biodegradable and do not contain nanoparticles. The development and implementation of ecologically sustainable adsorption technologies can help to overcome the challenges of water pollution and water scarcity in a cost-effective and energy-efficient manner.

Pectin, a polysaccharide present in the cellular walls of plants, has been used to remediate water against mono-, di-, and trivalent heavy metals (such as Zn^{2+}, Ni^{2+}, and Cd^{2+}) with high efficiency and the

* Corresponding author at: Centro de Física de Materiales (CSIC, UPV/EHU)-Materials Physics Center (MPC), Paseo Manuel de Lardizabal 5, San Sebastián 20018, Spain.
E-mail address: Silvina.cerveny@ehu.es (S. Cerveny).

https://doi.org/10.1016/j.cej.2023.146162
Received 5 June 2023; Received in revised form 5 August 2023; Accepted 18 September 2023
Available online 19 September 2023

possibility of reusing the adsorbent [4–6]. Pectin-based adsorbents must be insoluble for use in water. Crosslinking with calcium ions is common to achieve this, although other metal ions have also been used. Divalent metal ions, such as Ca^{2+}, promote the gelation of pectin [7]. The crosslinks are established between the carboxylate groups (COO^-, i.e., non-methyl-esterified residues) of neighboring pectin chains via the Ca^{2+} ions, which replace the hydrogen bonds in neat pectin. The degree of crosslinking in pectin is related to its degree of methoxylation (D_M), which represents the proportion of methyl-esterified carboxyl groups ($COOCH_3$) in comparison to non-esterified carboxyl groups (COOH) within the poly(galacturonic) chains at the carbon 6 position. Pectin with a low D_M demonstrates a more efficient crosslinking behavior. A sequence of non-methyl-esterified units between the 6 [8] and 20 [9] is necessary for the formation of these dimers. This structure is called the "egg-box" model and was first developed for alginates [10] and applied to low-D_M pectin [11]. Later [12,13], it was suggested that Ca^{2+} ions could also establish mono-complexes; that is, Ca^{2+} ions can interact with single carboxylate groups. Some reviews have summarized the formation of the "egg-box" model or other possible structures in pectin [7,14]. In addition to Ca^{2+}, pectin can also be reticulated by cations such as Zn^{2+}. Crosslinking with Zn^{2+} results in a more heterogeneous network structure because it interacts with both carboxyl and hydroxyl groups, whereas Ca^{2+} interacts only with carboxyl groups [15].

The main limitation of pectin-based adsorbents is that they are useful only for the removal of heavy metals and no other contaminants, such as pharmaceuticals and other emerging pollutants. To address this, we aimed to use Eu to crosslink pectin to enhance the removal of pharmaceutical products. Eu is a lanthanide that reacts with different pharmaceuticals [16,17]. It has been used as a fluorescent probe to detect hydrochlorothiazide (a diuretic drug) [17] and tetracycline (TC; an antibiotic) [18]. The interactions between pharmaceuticals and Eu can also be used for other purposes, such as that presented herein. It is also important to note that the acute toxicity of Eu was recently studied by Destefani et al. [19]. Eu was classified as a "category 4" material, which means that Eu has low toxicity when used in deficient concentrations, as those employed in this work.

This paper presents the innovative use of Eu as a crosslinking agent to enhance the performance of pectin-based adsorbents for water remediation. We developed a dual-crosslinking system that utilizes both Ca^{2+} and Eu^{3+} ions. We first investigated the isotherms and adsorption kinetics of pectin crosslinked with Ca^{2+} and Eu^{3+} separately to determine whether Eu^{3+} could be an effective reticulating agent. We then evaluated a dual-crosslinking system (Ca^{2+}+Eu^{3+}) and found that both agents effectively crosslinked pectin. Additionally, we assessed the swelling properties and the interaction between Eu and pharmaceuticals using fluorescence spectroscopy. We also compared the adsorption capacities of the adsorbents using three crosslinking systems (Ca^{2+}, Eu^{3+}, and the dual Ca^{2+}+Eu^{3+} system) for heavy metals (zinc) and two antibiotics (TC, and Ciprofloxacin (CIP)). When crosslinked with the dual system, pectin exhibited excellent adsorbent qualities for the simultaneous removal of heavy metals and pharmaceutical products.

2. Materials and methods

2.1. Materials

Low-methoxyl pectin (D_M = 9.9%) was sourced from Herbstreith & Fox. Glycerol, calcium chloride, sodium hydroxide, and europium chloride hexahydrate (product number 203254) were purchased from Merck and used without further purification. According to viscosimetry measurements, the molecular weight (M_w) of pectin was 82,000 g/mol (see Supplementary Material).

2.2. Preparation of pectin-based films

A 6% w/v glycerol and 3% w/v pectin solution was prepared in an Erlenmeyer flask under vigorous magnetic stirring at a temperature of 70 ℃ until homogeneous dissolution (1.5 h). The solution was then ultrasonicated at 70 ℃ for 1.5 h to homogenize the solution and eliminate bubbles. The solution (10 mL) was casted into a Petri dish and dried in a vacuum oven for 12 h. Finally, thin hydrogels were obtained, dried in a vacuum oven at 40 ℃, and stored until further use.

2.3. Crosslinking methods

Three crosslinking procedures were performed for a film dose of 2.5 g/L.

2.3.1. Ca^{2+} crosslinking

Pectin films were crosslinked using calcium chloride ($CaCl_2$). The dried pectin films were immersed in a 500 mg/L Ca^{2+} solution for 40 min.

2.3.2. Eu^{3+} crosslinking

Pectin films were crosslinked using europium chloride ($EuCl_3$). The dried pectin films were immersed in a 500 mg/L Eu^{3+} solution for 40 min.

2.3.3. Ca^{2+}+Eu^{3+} dual-crosslinking

The dried pectin films were crosslinked with Ca^{2+} and Eu^{3+} by immersing them in a 500 mg/L Ca^{2+} solution for 40 min followed by immersion in a Eu^{3+} solution for 40 min.

2.3.4. Post-crosslinking processing

For all three cases, after crosslinking, the films were rinsed five times with 200 mL of deionized water for 1 h to remove excess crosslinking agent. Thus, we obtained three pectin films with different crosslinking systems: P–Ca (samples crosslinked by Ca^{2+}), P–Eu (samples crosslinked by Eu^{3+}), and P–Ca + Eu (samples with dual-crosslinking by Ca^{2+} and Eu^{3+}).

To study the crosslinking reaction, we performed isotherm and adsorption kinetic studies as described below.

2.4. Characterization techniques

2.4.1. Fourier-transform infrared spectroscopy

Fourier-transform infrared (FT-IR) spectra were recorded on a Jasco FT/IR-6300 spectrometer (Japan) from 4000 to 600 cm^{-1} with a resolution of 4 cm^{-1} and 200 scans per spectrum in the attenuated total reflectance mode. All samples were dried at 40 ℃ in a vacuum oven prior to measurements to ensure a constant water content in all samples.

2.4.2. Scanning electron microscopy

The morphology and composition of the pectin-based adsorbents were investigated using scanning electron microscopy (SEM; Quanta 250 ESEM, FEI, Netherlands) and energy dispersive X-ray (EDX) spectroscopy (silicon drift detector, EDAX). The beam voltage and current were set to 10 kV and 5 pA, respectively. Electrons were detected using a large-field detector in low-vacuum mode. The chamber was evacuated to 80 Pa. The samples were mounted on an aluminum stub using double-sided tape.

2.4.3. X-ray diffraction

The dried neat pectin and crosslinked pectin films were characterized by powder X-ray diffraction (XRD; Philips X'pert PRO automatic diffractometer) using Cu Kα radiation (λ = 1.5418 Å) with a secondary monochromator and PIXcel solid-state detector. The voltage and current were 40 kV and 40 mA, respectively. The scans were performed with a 0.026 step size in the 2θ range of 2°–80° at room temperature. The percentage crystallinity was calculated as (crystalline area/total area) × 100.

2.4.4. Swelling experiments

The crosslinked pectin films were cut, accurately weighed, and placed in vials containing 100 mL of water (pH = 7) under agitation at room temperature. The films were weighted at certain intervals, after drying the surface water with filter paper. The same sample was used for each immersion time. The water uptake percentage was calculated as $(100 \times (M_{swollen} - M_{dry}))/M_{dry}$, where $M_{swollen}$ is the mass of the film after the water immersion, and M_{dry} stands for the mass of the dried film before the water immersion.

2.4.5. Inductively coupled plasma–atomic emission and ultraviolet–visible spectrometry

Inductively coupled plasma–atomic emission spectrometry (ICP–AES; Agilent 5100) was used to measure the equilibrium concentrations of heavy metals. The pharmaceutical concentrations were determined using ultraviolet–visible (UV–Vis) spectrometry (Agilent 8453A).

2.4.6. Contact angle

Contact Angle meter OCA 15 Plus, Data Physics Instruments GmbH, Filderstadt, Germany, equipped with a high-resolution CCD camera and a high-performance digitizing adapter, was used to determine the wettability of pectin films before and after remediation. A 3 µl droplet of distilled H_2O was placed onto the surface of the crosslinked pectin. SCA20 software (Data Physics Instruments GmbH, Filderstadt, Germany) was used for image capturing and contact angle determination.

2.4.7. Photoluminescence

Photoluminescence spectra were obtained using a Cary Eclipse Spectrophotometer (Agilent Technologies), with an excitation wavelength of 365 nm and slits of 5 nm.

2.5. Batch adsorption experiments

Adsorption isotherm and kinetic experiments were performed for two purposes. First, the crosslinking reactions with the three agents were monitored to determine the maximum adsorption capacities and appropriate crosslinking levels for each sample. Second, the experiments helped to analyze the adsorption of heavy metals and pharmaceuticals.

2.5.1. Crosslinking reactions

Adsorption isotherms were obtained using adsorbents with different initial Ca^{2+} or Eu^{3+} concentrations in the range of 25–1500 mg/L. A fixed amount of adsorbent (2.5 g/L) was used for each measurement. Batch experiments were performed in 20 mL tubes, and the equilibrium concentration was measured after 24 h. Kinetic adsorption studies were performed at a fixed crosslinking agent concentration (500 mg/L) for different durations (10 to 1440 min). Crosslinking solutions were prepared from $CaCl_2$ or $EuCl_3$, and the pH was maintained at 7 by adding 0.1 M NaOH.

2.5.2. Adsorption of heavy metals and pharmaceuticals

Similar experiments were performed to study the adsorption capacity of Zinc, two antibiotics (TC, and CIP). We used 1000 mg/L of a Zn^{2+} standard solution for ICP (18562, Sigma Aldrich) and deionized water for zinc dilutions. The three adsorbents were crosslinked for 40 min at a dose of 2.5 g/L.

Adsorption experiments were performed in batches using a dose of 2.5 g/L under agitation at 125 rpm and (25 ± 1) °C. Adsorption isotherms were measured at various initial pollutant concentrations. For the kinetic experiments, we measured the pollutant concentration at different times ranging from 10 to 1440 min at a fixed initial concentration of 150 mg/L for zinc and at 50 mg/L for the pharmaceuticals.

In both the cases, the equilibrium concentration (C_{eq}) and concentration at time t (C_t) were measured using ICP–AES; for the pharmaceuticals, UV–Vis was used to measure C_{eq} and C_t. The amount of adsorbed crosslinking agent or pollutant was determined based on the difference between the initial and final concentrations in the solution. Aliquots were collected at certain intervals to measure C_t, and C_{eq} was taken as the equilibrium value of C_t. The equilibrium adsorption capacity (q_{eq}; mg/g) and adsorption at time t (q_t; mg/g) were calculated as follows:

$$q_{eq} = \frac{C_0 - C_{eq}}{d} \tag{1}$$

$$q_t = \frac{C_0 - C_t}{d} \tag{2}$$

where C_0 is initial concentration of a given crosslinking agent or pollutant (mg/L) and d (g/L) is the adsorbent dose. The removal efficiency (R%) was calculated as follows:

$$R\% = \left(\frac{(C_0 - C_{eq})}{C_0}\right) \times 100\% \tag{3}$$

2.5.3. Reusability studies

For regeneration and reusability studies, pectin films were subjected to five adsorption cycles (dose of 2.5 g/L), each followed by one desorption. Solutions of 10 mg/L of Zinc and 50 mg/L of Tetracycline or Ciprofloxacin at pH 7 were used for adsorption. The final concentration was measured after 2 h. Desorption was performed for 1 h using nitric acid 0,1 M to desorb Zinc. We used formic and acetic acids at 1% for TC and CIP. Desorption and adsorption were done under orbital shaking at 120 rpm. A washing and drying step in water between adsorption–desorption is required to remove the excess reagents.

2.6. Adsorption data analysis

The adsorption isotherms were fitted using the Langmuir (Eq. (4) and Redlich–Peterson (Eq. (5) models [20].

$$q(C_{eq}) = \frac{q_M K_L C_{eq}}{1 + K_L C_{eq}} \tag{4}$$

$$q(C_{eq}) = \frac{K_{RP} C_{eq}}{1 + \alpha C_{eq}^{\beta}} \tag{5}$$

where q is the adsorption capacity; q_M is the maximum adsorption capacity; K_L is the Langmuir constant; and KL_{RP}, β, and α are Redlich–Peterson constants. β is a dimensionless parameter between 0 and 1, representing the heterogeneity factor. The closer the value to zero, the more heterogeneous the surface where the adsorbate interacts.

The adsorption data were analyzed using a nonlinear fitting of the empirical pseudo-first-order (PFO; Eq. (6)) and pseudo-second-order (PSO; Eq. (7)) kinetic models [21].

$$\text{PFO}: q_t = q_e(1 - e^{-k_1 t}) \tag{6}$$

$$\text{PSO}: q_t = \frac{q_e^2 k_2 t}{1 + q_e k_2 t} \tag{7}$$

where k_1 and k_2 are the characteristic time-related constants of the PFO and PSO models, respectively, indicating the adsorption speed at the beginning of the adsorption process.

3. Results and discussion

3.1. Crosslinking reactions

3.1.1. Isotherms

This section presents the isotherms (24 h) of pectin crosslinked using Ca^{2+}, Eu^{3+}, and the dual- Ca^{2+}+Eu^{3+} crosslinking system. Hereinafter, these systems are denoted as P-Ca, P-Eu, and P-Ca-Eu, respectively.

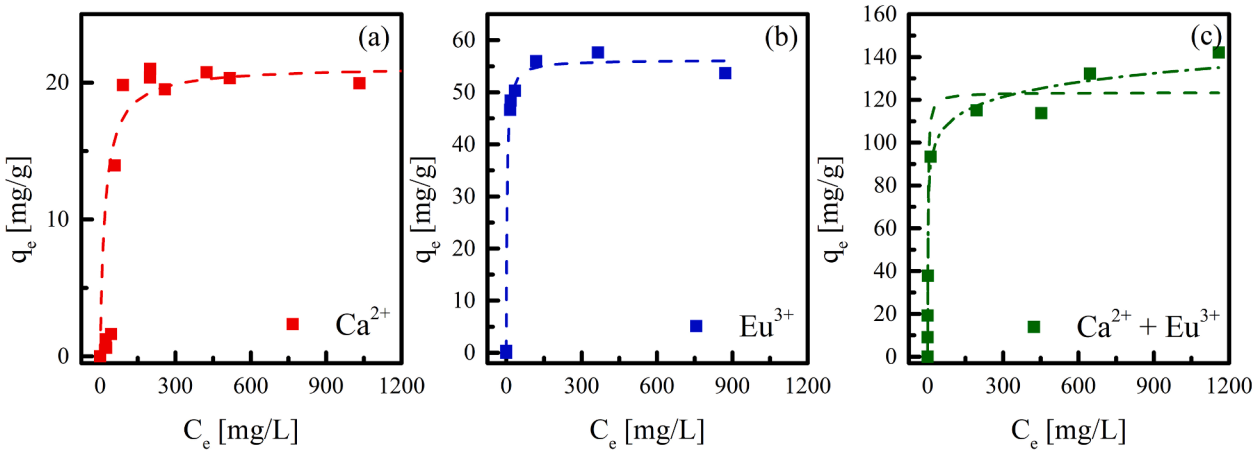

Fig. 1. Adsorption isotherms of pectin films (dose of 2.5 g/L) at pH = 7 using (a) Ca, (b) Eu, and (c) Ca + Eu as the crosslinking agents. The dashed lines in panels (a)–(c) indicate the nonlinear fittings obtained using the Langmuir model, and the dotted–dashed line in panel (c) indicates the nonlinear fitting obtained using the Redlich–Peterson model.

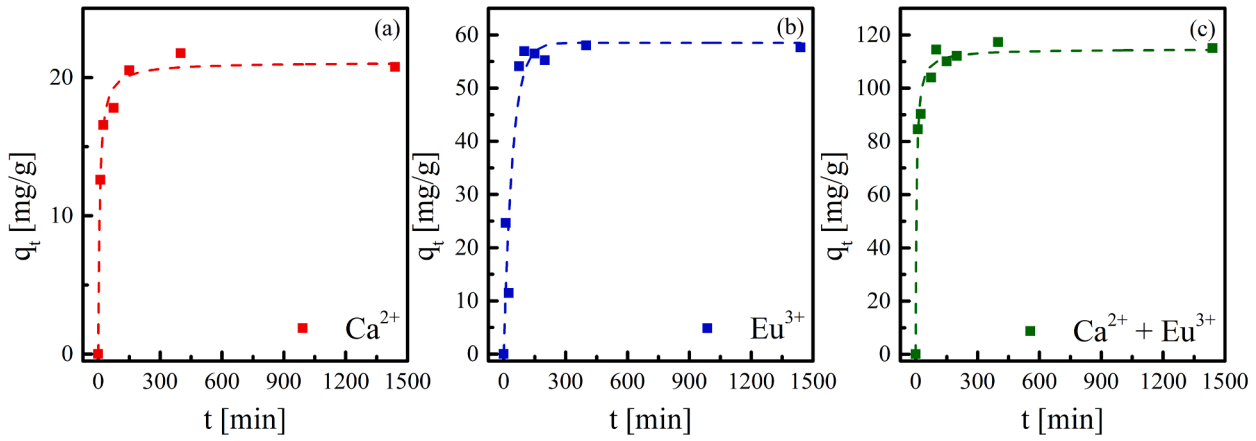

Fig. 2. Adsorption kinetics of pectin films (dose of 2.5 g/L) at pH = 7 using (a) Ca, (b) Eu, and (c) Ca + Eu as crosslinking agents. The dashed lines indicate the nonlinear fittings obtained using the PSO and PFO models.

Fig. 1a and b show the Ca and Eu adsorption capacities of pectin after 24 h as a function of the equilibrium Ca and Eu concentrations, respectively, and Fig. 1c shows the Eu adsorption capacity of the film crosslinked with Ca. The adsorption capacities increased with increasing initial Ca or Eu concentration until a plateau value was reached.

As shown in Fig. 1 and Table 1, the maximum adsorption capacity of pectin for Ca was approximately 21 mg/g, whereas that for Eu was 56 mg/g. In contrast, the adsorption capacity of the Ca-crosslinked pectin for Eu increased to 140 mg/g. Thus, the ability to adsorb Eu more than doubled after Ca-crosslinking. It can be concluded that the dual-crosslinking system promoted the adsorption of Eu by the pectin film.

The isotherms for pectin crosslinked with Ca or Eu were fitted using the Langmuir model (Table 1). This model assumes that adsorption occurs at identical sites and that only one molecule can be adsorbed at each location [20,21]. For the sample reticulated with the dual system, the isotherm was fitted using both the Langmuir and Redlich–Peterson models [22]. The Redlich–Peterson model had a better fit ($R^2 = 0.99$), which implies that this system does not exhibit ideal monolayer adsorption behavior; the adsorption sites can be homogeneous or heterogeneous and are not identical [23]. This indicates that the structures of the samples crosslinked with Ca or Eu differ from those reticulated with both Ca and Eu. Regarding the parameters obtained from the fitting, the K_L and K_{RP} values indicate that the extent of the interaction between the adsorbate and adsorbent is favorable.

3.1.2. Kinetics

We analyzed the adsorption kinetics of pectin during crosslinking using the three agents. Fig. 2 shows the results of crosslinking with the three agents as a function of adsorption time. The isotherms show that the Eu uptake in the dual-crosslinking system was very high compared

Table 1
Calculated adsorption parameters for the three types of pectin film using the Langmuir and Redlich–Peterson adsorption isotherm models.

Sample	Model	R^2_{adj}	K_L [L/mg]	K_{RP} [L/mg]	q_{Max}[a] [mg/g]
P–Ca	Langmuir	0.99	0.050 ± 0.032	—	21.2 ± 0.6
P–Eu	Langmuir	0.99	0.32 ± 0.06	—	56.2 ± 0.9
P–Ca-Eu	Langmuir	0.96	0.65 ± 0.26	—	123.4 ± 5.4
P–Ca-Eu[b]	Redlich–Peterson	0.99	—	139.2 ± 39.7	

[a] q_{Max} is the maximum adsorption capacity. [b]For pectin–Ca^{2+}+Eu^{3+} using the Redlich–Peterson model, $\alpha = 1.78 \pm 0.64$ mg/L and $\beta = 0.92 \pm 0.02$.

Table 2
Calculated kinetic parameters for the three types of pectin film using PFO or PSO adsorption models.

Sample	Model	R^2_{adj}	k_1 [L/min]	k_2 [g/(mg min)]	q_{eq} [mg/g]
P–Ca	PSO	0.99	——	0.0064 ± 0.0013	21.1 ± 0.5
P–Eu	PFO	0.89	0.024 ± 0.007	——	58.5 ± 4.0
P–Ca + Eu	PSO	0.99	——	0.0020 ± 0.0004	114.7 ± 2.1

with that in the case with Eu alone.

To select an appropriate kinetic model (PFO or PSO) and understand the ion adsorption mechanism, we used three criteria: the R^2 value extracted from the linear fitting, Akaike criterion, and Bayesian criterion [24]. Based on the results (see the complete calculations in the Supplementary Material), the crosslinking reactions of pectin with Ca and the dual system (Ca + Eu) were best fitted using the PSO model, indicating that the adsorption process was driven by chemisorption [25]. In contrast, the crosslinking reaction with Eu was best fitted using the PFO model, indicating that the adsorption process was driven by electrostatic interactions or physisorption rather than chemisorption [26,27]. Fig. 2 and Table 2 show the fitting results. Thus, we can conclude that the samples crosslinked with Ca and the dual system (Ca + Eu) had stronger interactions between the ions and pectin than those crosslinked only with Eu.

3.2. Morphology

Fig. 3a–d shows SEM images of the untreated and crosslinked pectin. Morphological changes can be observed after crosslinking with the three agents. P–Ca had a spherical granular shape with a homogeneous size, whereas P–Eu had a more granular surface with a preferential orientation. In contrast, P–Ca + Eu presented a more uniform surface than neat pectin.

The EDX spectra in Fig. 3 indicate that all the crosslinked samples contained Ca or Eu (see element content in Table S2 of SM). Neat pectin contained Na (Fig. 3a), favoring the reticulation reaction [28]. After crosslinking with Ca (Fig. 3b) or Ca + Eu (Fig. 3d), a peak was detected at 3.70 keV, indicating the presence of Ca, and after crosslinking with Eu (Fig. 3c) or Ca + Eu (Fig. 3d), two peaks related to Eu were detected at 1.13 and 5.8 keV. These peaks confirmed the existence of crosslinking in all three cases. The EDX spectra did not exhibit significant variations in different sections of the samples, indicating a homogeneous dispersion of Ca, Eu, or both.

3.3. Structural properties of different crosslinked pectin-based adsorbents

In this section, we analyze the structural properties of the three crosslinked samples. Fig. 4a shows the infrared spectra of the neat and crosslinked pectin samples used to determine the structural differences between the three crosslinking agents. The intense band in the region of ~3600–3000 cm^{-1} corresponds to the stretching of hydroxyl groups (–OH), whereas the bands in the region of 3000–2850 cm^{-1} represent methyl vibrations ($–CH_3$). The band at ~ 1725 cm^{-1} corresponds to the C = O stretching of nonionic carboxyl groups (–COOH, $–COOCH_3$), whereas the band at ~ 1610 cm^{-1} is assigned to the asymmetric stretching vibrations of carboxylate anions (COO^-) [29,30].

The most significant changes after crosslinking were observed in the carboxylate anion band (~1600 cm^{-1}). In particular, the band at 1591

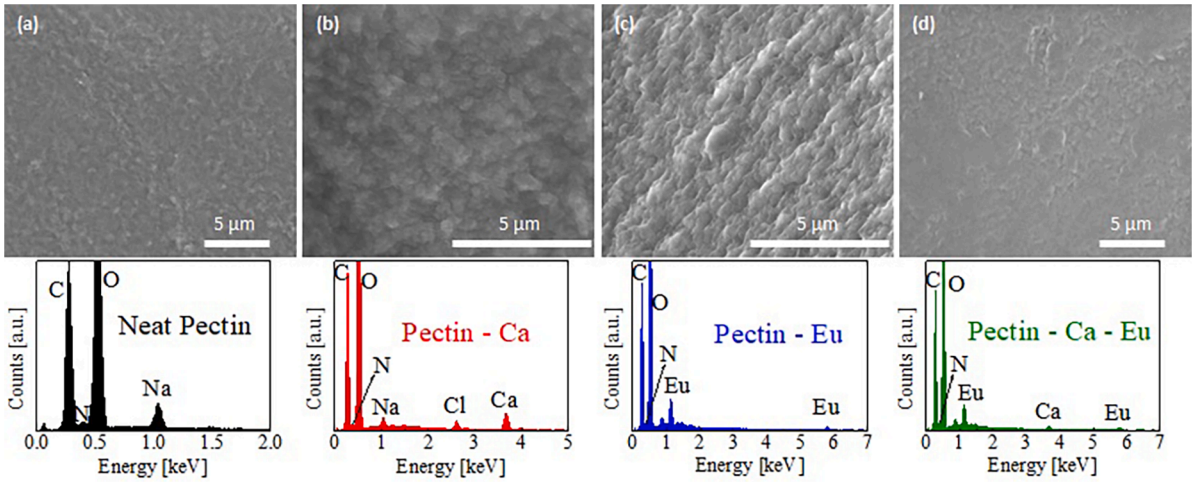

Fig. 3. Scanning electronic microscopy images and EDX spectra of pectin-based films with (a) neat pectin and pectin samples crosslinked with (b) Ca, (c) Eu, and (d) Ca + Eu. Fig. S3 shows images of the regions used for EDX mapping.

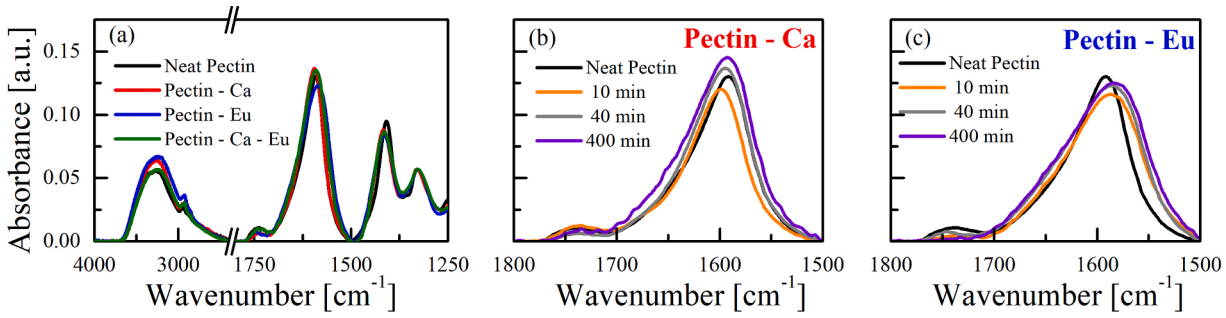

Fig. 4. Infrared spectra of (a) neat and crosslinked pectin using three different crosslinking agents and (b) P–Ca and (c) P–Eu films crosslinked for different durations (10, 40, and 400 min).

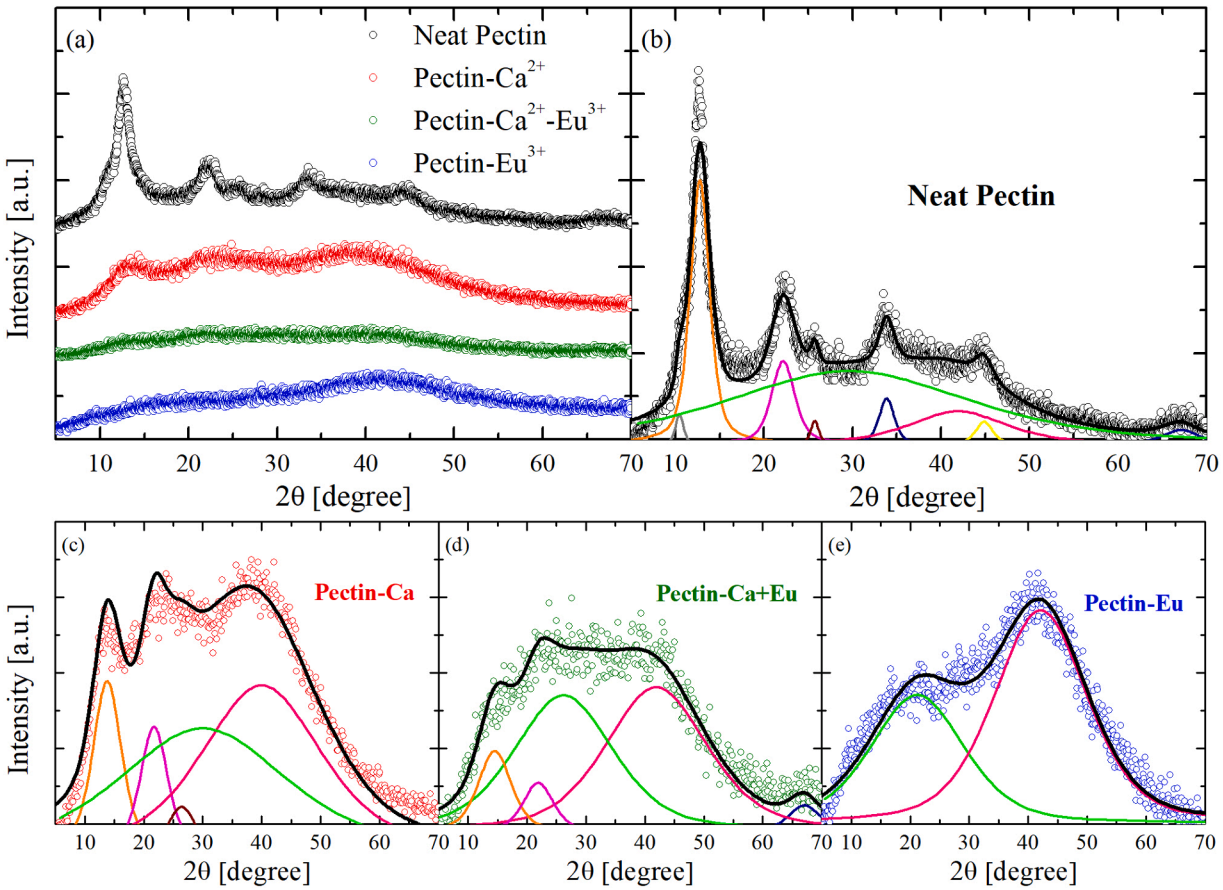

Fig. 5. (a) Comparison of the XRD patterns of pectin adsorbents using different crosslinking agents. (b–d) XRD patterns of neat and crosslinked pectin films. Experimental data are indicated by points, and fittings of the experimental data with the pseudo Voigt profiles are indicated by solid lines.

cm^{-1} for neat pectin shifted to 1598 cm^{-1} upon crosslinking. This shift to higher wavenumbers has been previously reported [28] and is because Ca ions strongly interact with the ionized carboxyl group. However, in the case of dual crosslinking, the band shifted slightly to 1590 cm^{-1}, and in the case of Eu crosslinking, the shift was much more evident to 1583 cm^{-1}. Therefore, unlike Ca, the Eu ions interact less with the ionized carboxylate group, which is most noticeable in the case of Eu alone. We confirmed this result by analyzing the crosslinking of pectin with Ca and Eu separately (not in the dual-crosslinking system) at different durations (10, 40, and 400 min). Fig. 4b and c show that, even in the first few minutes of the crosslinking reaction, the Eu ions interact less with the ionized carboxylate group (Fig. 4c). This suggests that it is difficult to rationalize the formation of an "egg-box" structure when pectin is crosslinked with Eu.

Further evidence of the structure of each crosslinking system can be found in the XRD patterns of the pectin films, as shown in Fig. 5. In particular, the XRD patterns provide information about the amorphous and crystalline phases in each material [31]. For the neat pectin film, the XRD pattern contained sharp crystalline peaks at 2θ values of 12.6°, 22.6°, and 33.8°, indicating a high degree of crystallinity (see the fitting procedure in Fig. 5b). Amorphous halos were observed at 2θ values of 31° and 41.9°, which do not produce a well-resolved XRD pattern and represent the amorphous fraction of neat pectin. From the most intense diffraction peak, a typical *d*-spacing of 0.70 nm was obtained for the neat pectin film, which agrees with previous reports [32].

After Ca crosslinking, the diffraction peaks were broader than those for the neat pectin film, indicating a lower degree of crystallinity. However, peaks at 2θ values of 14°, 23.7°, and 27.0° were observed with amorphous halos at 2θ values of 30° and 40°. Considering the most intense diffraction peak, a typical *d*-spacing of 0.63 nm was obtained for the Ca-crosslinked pectin film, indicating a variation in the lateral spacing between pectin chains between the untreated (0.70 nm) sample and the Ca-crosslinked one (0.63 nm). This XRD pattern has been previously reported for the dimerization of polymer chains through Ca coordination, according to the egg-box model [33,34].

The Ca + Eu-crosslinked sample had even lower crystallinity, as the diffraction peaks were even broader than those of the sample reticulated with Ca. Nevertheless, we could still distinguish between the peaks at 2θ values of 14.5° and 21.0°, with broad peaks at 2θ values of 26° and 41°. Considering the diffraction peak at 14.5°, a typical *d*-spacing of 0.61 nm was obtained. Thus, the interlayer distance systematically decreased for the neat pectin, P–Ca, and P–Ca + Eu samples, while the peaks became broader and less intense. Moreover, using the integration method, we estimated the crystallization percentages to be 34%, 21%, and 15% for neat pectin and the Ca and Ca + Eu reticulated samples, respectively. This indicates that after adding Eu, the sample lost half its crystalline phase, and gradual amorphization of the pectin was observed when the crosslinking changed from Ca to Ca + Eu.

In contrast, after crosslinking pectin with Eu alone, the XRD pattern only showed amorphous halos centered at 2θ values of 21° and 42°, indicating highly defective crystals, if any. In addition, the crystalline fraction was reduced to zero. Thus, crosslinking with Eu alone induced complete amorphization of the pectin; consequently, we could not find any signs of the "egg-box" model when the sample was crosslinked with Eu.

In the absence of divalent cations, pure pectin chains interact via hydrogen bonds [9]. In the presence of Ca ions, the pectin chains interact via noncovalent Ca bridges between the carboxyl groups of two different chains (dimerization [35]) and the hydrogen bonds that remain in the network [36]. These results were reflected in the FT-IR and XRD

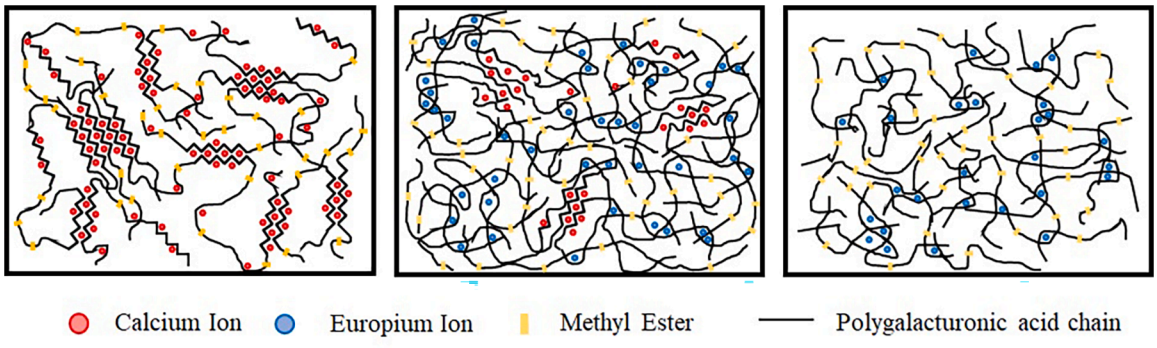

Fig. 6. Schematics of three crosslinked systems: (a) P–Ca (a), (b) P–Ca + Eu, and (c) P–Eu.

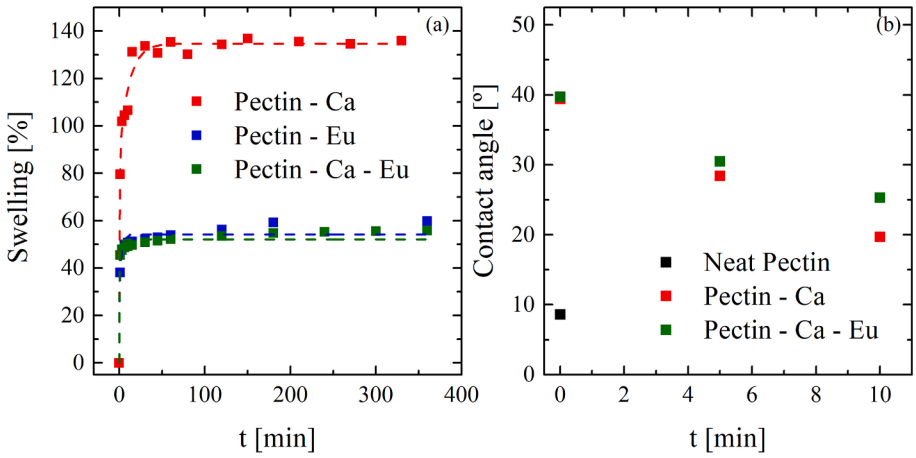

Fig. 7. (a) Swelling properties of pectin crosslinked with Ca, Eu, and Ca + Eu. (b) Contact angle of pectin-based adsorbents.

results. When Eu atoms enter the P–Ca lattice, they introduce defects into the periodic network, as evidenced by the loss of crystallinity and reduced interaction between the carboxylate groups. However, at this point, we could not confirm whether, for this sample, there was only a break of periodicity when Eu entered the network or whether there was a disassembly of the "egg-box" structure.

To assess this further, we performed ICP–AES experiments to analyze the release of Ca ions when the sample was further crosslinked with Eu. After Ca crosslinking, the P–Ca films were washed extensively (100 mL of water, 1 h each under agitation, five times). The water from each wash cycle was analyzed by ICP to determine whether some of the Ca ions were released (i.e., not bound to the pectin chains). Furthermore, we investigated whether, in the dual-crosslinking system, there was ion exchange between Ca and Eu (i.e., to determine if, during Eu crosslinking, some of the Ca ions were released from the sample). The results showed that, during Eu crosslinking, almost 70% of the Ca ions were released. Therefore, Eu disassembled much of the "egg-box" structure, as most of the Ca ions were lost. For example, considering P–Ca crosslinked for 40 min, the Ca uptake was 2.69×10^{-5} mol, and during Eu crosslinking, the sample released 1.77×10^{-5} mol Ca. This indicated that the sample lost 67% of the Ca ions.

The sample crosslinked with only Eu lost all its crystallinity, indicating an amorphous sample with less interaction between the carboxyl groups. The established crosslinks could be point-like interactions between two or three chains, enabling the formation of a stable 3D network. Fig. 6 schematically shows the expected structures of pectin using three different crosslinking agents based on the SEM, XRD, and FT-IR results. We expected an egg-box model for P–Ca, in which two carboxyl groups are attached to each Ca ion. Conversely, Eu formed an amorphous network with random crosslinking points, as shown in Fig. 6c. Finally, the dual-crosslinked sample with Eu and Ca exhibited both crystalline and amorphous phases, as shown in Fig. 6b.

3.4. Swelling of pectin adsorbents

The diverse structures of the different crosslinking systems also affected the swelling properties (Fig. 7). This property is relevant in water treatment because pollutants reach adsorption sites after diffusing

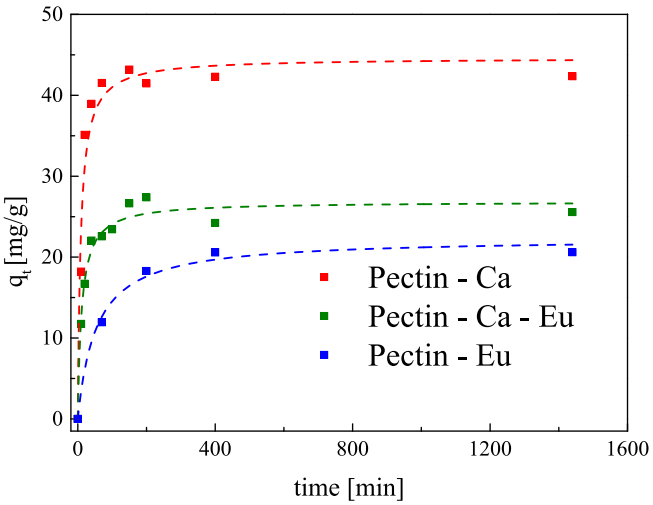

Fig. 8. Kinetics of Zn^{2+} sorption by pectin crosslinked with Ca, Eu, and Ca + Eu. Adsorbent dose: 2.5 g/L, initial Zn^{2+} concentration: 150 ppm. Dashed lines represent the fitting of the PSO model (see Table 3).

Table 3
PSO kinetic parameters for Zn^{2+} sorption into P–Ca, P–Eu, and P–Ca + Eu. MRE represents Maximum removal efficiency.

Sample	R^2_{adj}	K_2 [g/(mg min)]	q_{max} [mg/g]	MRE[%]
P–Ca	0.96	0.0026 ± 0.0007	44.6 ± 1.6	75.0
P–Ca + Eu	0.98	0.0032 ± 0.0006	26.9 ± 0.7	47.2
P–Eu	0.99	0.0008 ± 0.0002	22.4 ± 0.9	37.9

into the matrix. As swelling depends on the sample size, all the measurements (average of three runs) were conducted using samples with similar dimensions (thickness 0.154 ± 0.031, 0.157 ± 0.015, and 0.141 ± 0.024 mm for P–Ca, P–Eu, and P–Ca + Eu, respectively).

The P–Ca films reached water uptake equilibrium after 2 h, whereas the P–Eu and P–Ca + Eu films reached equilibrium very quickly (after 15 min). The P–Ca film was also the most swollen system, whereas P–Eu and P–Ca + Eu had less affinity for water. This indicates that there were more available hydroxyl, carboxyl, and carboxylate groups in Ca-crosslinked pectin to establish H-bonds with water than in the Eu and Ca + Eu films.

In addition, to assess the hydrophilicity behavior of the film surfaces, we studied the contact angles of the P-Ca and P-Ca-Eu films (see Fig. 7b). Initially, both films exhibited similar contact angles, approximately 40°. This indicates comparable hydrophobicity in their dry state. It has been reported that surface roughness affects the contact angle of surfaces. Moreover, an increase in surface roughness can lead to higher hydrophobicity. In Fig. 3, we observed that P-Ca exhibited a spherical granular shape, suggesting that its morphology might contribute to its seemingly higher hydrophobicity than reality. However, after 10 min, the contact angle for P-Ca-Eu was higher (25.3°) than that for P-Ca (19.7°). This result indicates that the water absorption capacity is higher for P-Ca films, which confirms the results in Fig. 7a.

3.5. Kinetics of Zn^{2+} and pharmaceutical sorption on three reticulated pectin adsorbents

This section focuses on the application of the developed adsorbents for water remediation. The pH of the contaminated water was maintained at 7 in the experiments because this is its natural pH. Pectin, with a low degree of esterification and crosslinking with Ca, is an excellent adsorbent for mono- and divalent heavy metals [4–6]. However, to the best of our knowledge, there are no reports on the adsorption of other emerging contaminants, such as pharmaceuticals using pectin-based adsorbents. It is also important to note that we have also analyzed the possible Eu release into the water before and after adsorption by ICP-AES. The results showed that no Eu was released into the water.

3.5.1. Non-simultaneous removal of heavy metals and pharmaceuticals

Fig. 8 shows the kinetic results (fitted with the PSO model; Table 3) for the adsorption of Zn^{2+} using the three adsorbents. The maximum removal efficiency decreased from 75% to 47.2% and 37.9% for Ca, Ca + Eu, and Eu, respectively. This was expected because there were fewer Ca ions in the P–Ca + Eu sample than in the P–Ca sample. The P–Eu sample was also able to adsorb Zn, although its removal efficiency was lower than that of the P–Ca adsorbent. The reason the P–Eu sample can adsorb Zn is unclear, but we expect it is because Zn can also crosslink pectin and not because of a strong interaction between Eu and Zn. Further studies will be required to confirm this hypothesis.

Fig. 9 shows the adsorption kinetics of the crosslinking systems for two pharmaceutical products: TC and CIP. P–Ca did not exhibit any adsorption capability for antibiotics. Given the high affinity of Eu for both TC and CIP [37,38], its removal ability is expected to be high.

Indeed, the P–Eu adsorbent had good sorption ability for TC and CIP, but it is still higher for the P-Ca-Eu adsorbent. This is because the Eu concentration was higher in the P–Ca + Eu sample than in the P–Eu sample (concentrations of Eu were determined by ICP-AES in section 3.1). Table 4 shows the fitting parameters corresponding to the PFO and

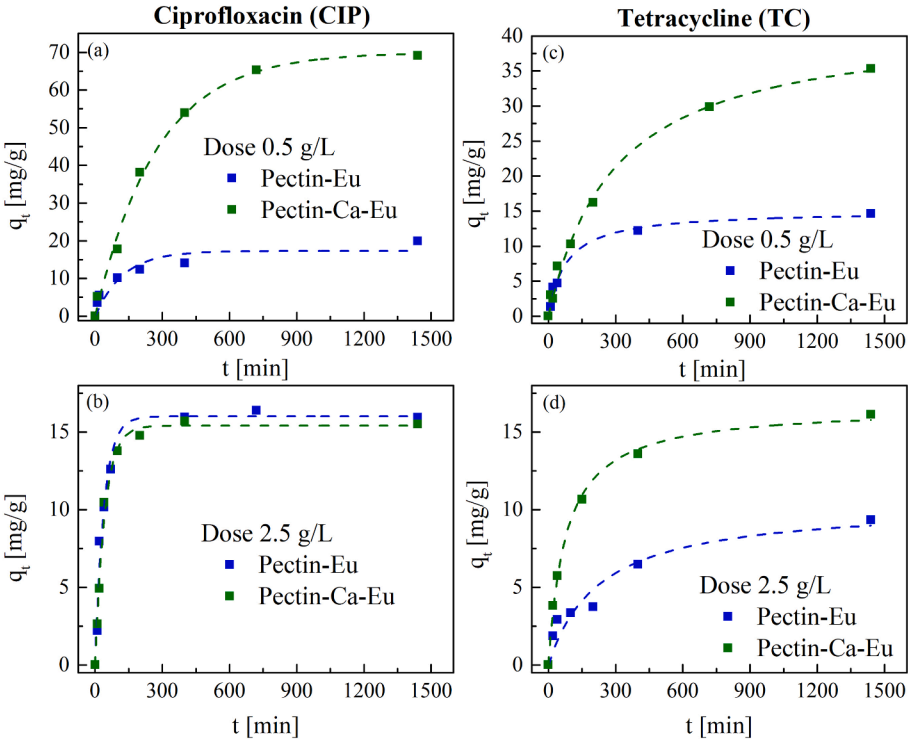

Fig. 9. Adsorption kinetics of P–Eu and P–Ca + Eu for (a and b): ciprofloxacin (CIP) at a dose of 2.5 g/L and 1 g/L respectively; (c and d): tetracycline (TC) at a dose of 0.5 g/L and 2.5 g/L, respectively. Initial adsorbate concentration: 50 ppm. Dashed lines represents the fitting of the PFO and PSO models (see Table 4).

Table 4
PFO kinetic parameters for TC and CIP sorption into P–Eu and P–Ca + Eu films at a dose of 0.5 g/L.

Sample	Ads[a]	Model	R^2_{adj}	k_1 [L/min)]	k_2 [g/(mg min)]	q_{max} [mg/g]	MRE[b] [%]
P–Eu	CIP	PFO	0.98	0.008 ± 0.002		17.4 ± 1.7	96
P–Eu	TC	PSO	0.89		0.0008 ± 0.0002	14.5 ± 1.5	48
P–Ca + Eu	CIP	PFO	0.99	0.0030 ± 0.0004		71 ± 3	91
P–Ca + Eu	TC	PSO	0.99		0.00008 ± 0.00001	34.6 ± 1.4	81

[a] Ads: adsorbate. [b]MRE: maximum removal efficiency (C_0 = 50 mg/L).

PSO models for samples with a dose of 0.5 g/L. Remarkably, the maximum removal efficiency, with a dose of 2.5 g/L, is high, 91 and 81 for CIP and TC, respectively.

Finally, we also studied the interaction mechanism between TC and CIP with P-Ca-Eu and P-Eu adsorbents. It has been previously studied that TC can form stable complexes with Eu via the β-diketone structure present in TC [39]. This complexation shows photoluminescence features, and therefore the Eu-TC interaction can be detected by fluorescence spectroscopy.

Fig. 10 shows the emission spectra generated by Eu and its complexes with TC and CIP adsorbed in P-Eu and P-Ca-Eu films (excitation wavelength 365 nm). Eu shows a fluorescence characteristic peak at 615 nm [40], as seen in the spectra corresponding to the films without antibiotics. After adsorption, the significant enhancement of the emission spectrum at 615 nm indicates the formation of the complexbetween Eu and β-diketone group on TC or CIP [41,42].

3.5.2. *Competitive adsorption: Simultaneous removal of pharmaceuticals and Zn^{2+}*

Typically, adsorption processes are studied using a single pollutant. However, water is usually polluted with several contaminants [43], which can have a negative or positive role in the adsorption process. For example, heavy metals can compete with pharmaceuticals for adsorption sites [44]. In the present case, we expect the heavy metals to interact with Ca ions and the pharmaceuticals to interact with Eu^{3+} or COO^- groups.

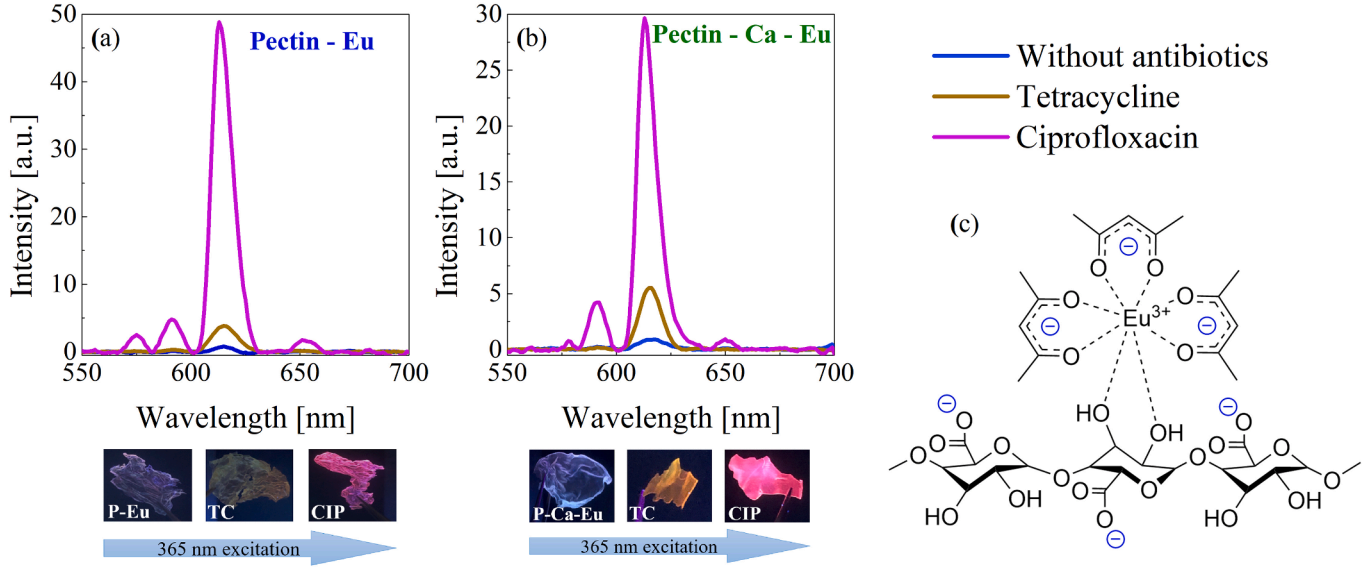

Fig. 10. Emission spectra generated by Eu and its complexes with TC and CIP adsorbed in (a) P-Eu and (b) P-Ca-Eu films (photos show the P-Eu and Pe-Ca-Eu films before and after TC and CIP adsorption under 365 nm UV irradiation). (c) Cartoon of the proposed mechanism for the interaction between TC and Eu or CIP and Eu.

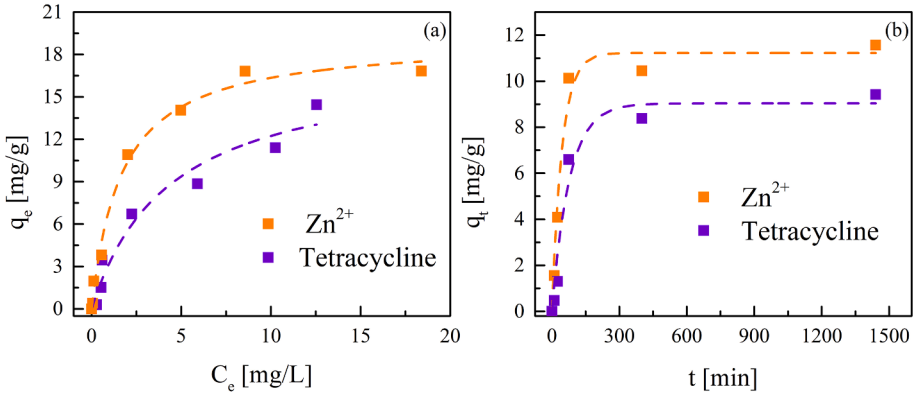

Fig. 11. (a) Adsorption isotherms and (b) kinetics of the simultaneous removal of Zn^{2+} and TC by P–Ca + Eu. Adsorbent dose: 2.5 g/L, initial Zn^{2+} and TC concentration: 30 ppm. Dashed lines represent the fitting of the Langmuir model (a) and PSO model (b) (see Table 5).

Table 5
Isothermal parameters of the Langmuir model and kinetic parameters of the PSO model for simultaneous Zn^{2+}/TC removal using P–Ca + Eu adsorbent.

	Isothermal parameters				Kinetic parameters			
Ads[a]	R^2_{adj}	K_L [L/mg]	q_e [mg/g]	MRE[b] [%]	R^2_{adj}	K_2 [g/(mg min)]	q_{max} [mg/g]	RE_{max} [%]
Zn^{2+}	0.99	0.60 ± 0.09	19.1 ± 0.8	94.5	0.98	0.004 ± 0.001	10.9 ± 0.4	93.3
TC	0.96	0.23 ± 0.09	17.6 ± 0.2	93.6	0.99	0.0007 ± 0.0001	9.7 ± 0.5	79.5

[a] Ads: adsorbate. [b]MRE: maximum removal efficiency (C_0 = 10 mg/L).

Table 6
Adsorption capacities of pectin-based adsorbents compared with literature-reported similar adsorbents.

Adsorbent	Ads.	Dose [g/L]	C_0 [mg/L]	q_{eq} [mg/g]	REF.
P - Ca	Zn^{2+}	2.5	150	44.6 ± 1.6	–
Calcium alginate beads	Zn^{2+}	2.5	100	53	[45]
Inula Viscose leaves	Zn^{2+}	1	50	13	[46]
P- Ca -Eu	CIP	1	50	70.0 ± 2.0	–
Cationic flax oil cellulose	CIP	0.4	80	188.67	[47]
Nickel alginate particles	CIP	0.5	20	33.76	[48]
P - Ca - Eu	TC	0.5	50	42.3 ± 1.9	–
Sodium alginate copper beads	TC	0.05	20	14.87	[49]
Iron(III)-loaded cellulose nanofibres	TC	0.5	10	19.20	[50]

Fig. 11 shows the isotherms and adsorption kinetics for the simultaneous removal of Zn^{2+} and TC by P–Ca + Eu films. The experiments were performed at an adsorbent dose of 2.5 g/L. The concentrations of the mixed pollutants (Zn^{2+} and TC) ranged from 1 to 60 mg/L, and the solution pH was adjusted to 7. The heavy metal and antibiotic concentrations were determined by ICP–AES and UV–Vis absorption spectroscopy, respectively.

The isotherms were fitted to the Langmuir model, which assumes that a chemical process occurs at homogeneous binding sites. We found a good removal efficiency of approximately 94% for Zn^{2+} and TC (Table 5). These results demonstrate that pectin combined with both Ca and Eu reticulation agents is a promising adsorbent for a combination of pollutants.

Finally, Table 6 compares the efficiency of the adsorbents developed in this work with other adsorbents using the same pollutants. As seen in the table, the Zn adsorption capacity of the P-Ca films and the ciprofloxacin adsorption capacity of the P-Ca-Eu films are within the range reported in the literature. On the other hand, the remediation of tetracycline by P-Ca-Eu film demonstrates significantly higher adsorption capacity than those found in the literature.

3.6. Reusability studies

Fig. 12 shows that pectin films can be reused after Zn, TC, or CIP adsorption. This information is crucial for escalation objectives as well as for the possible impact produced on the environment. Moreover, our previous studies (not shown here) demonstrate that one hour was enough time for desorption, which is a quick time for industrial purposes.

The desorption efficiency (R_{des}%) was calculated as follows:

$$R\% = \left(\frac{C_{des}}{(C_0 - C_{ads})}\right) \times 100\% \quad (8)$$

where C_{des} is the concentration of the desorbed pollutant after 1 h, and C_{ads} is the concentration after 2 h of adsorption.

The adsorption efficiency of Zn in the P-Ca-Eu film treated with nitric acid remained consistent across all 5 cycles, ranging from 84% to 89%. However, the desorption efficiency dropped to 80% during the fifth cycle, indicating that the pectin film lost effectiveness after the fourth cycle.

In the case of desorption of antibiotics, we prefer using organic green acids (acetic and formic acids) with lower pKa than nitric acid because they can interact more selectively in the system without significantly

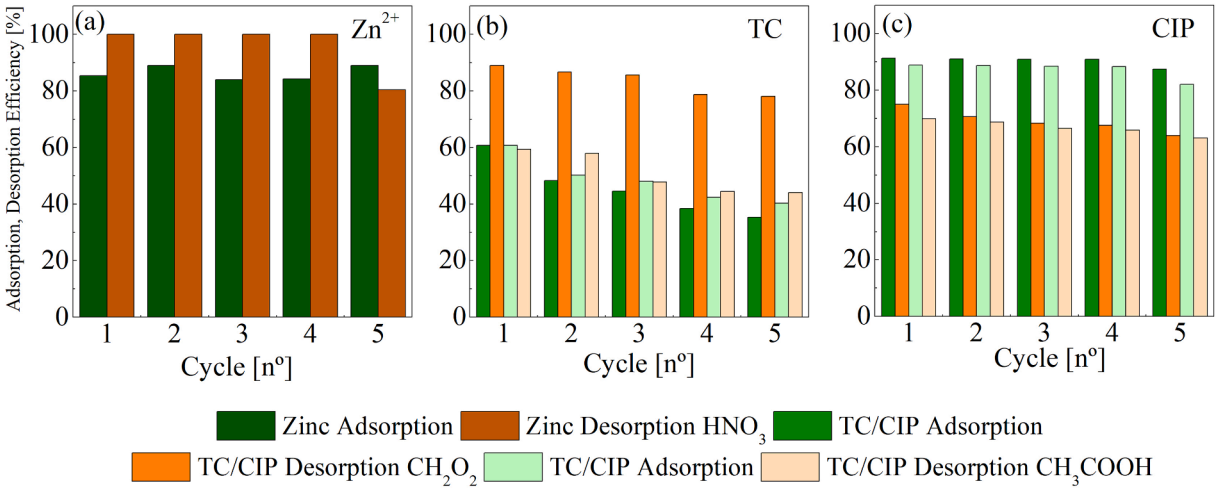

Fig. 12. Relative adsorption efficiency of Zn (a), TC (b) and CIP (c) in pectin films on each adsorption cycle, followed by regeneration. TC and CIP desorption was done with acetic acid (CH_3COOH) and with formic acid (CH_2O_2), whereas Zn was desorbed with nitric acid (HNO_3).

losing performance after 5 cycles. Formic acid has more intense desorption activity than acetic acid due to its higher pKa.

TC in P-Ca-Eu films shows lower removal efficiency than CIP-containing samples due to their different kinetics (see Fig. 9). The sample containing TC treated with formic or acetic acids decreased its removal efficiency throughout the process. However, after the fourth cycle, the sample containing CIP shows a slight reduction in removal efficiency. This difference is probably related to a stronger interaction between Eu and TC complex compared with CIP.

Regarding the desorption cycles, we observe a lower efficiency for TC than CIP, independently of the acid used. We believe that we are losing the Eu-TC complex during the acid treatments. However, CIP did not show this behavior because the removal efficiency remains constant throughout the desorption cycles. Therefore, we conclude that TC cannot be recovered from pectin films, whereas CIP can be effectively recovered.

4. Conclusions

Strict environmental regulations on water quality both in the EU and the rest of the world have increased the need to improve the quality of treated wastewater, particularly considering the emerging contaminants (among others, heavy metals and pharmaceuticals). Pectin is a promising adsorbent for water remediation because it is cost-effective and environmentally friendly. However, it can currently only be used for heavy metal removal.

Here, a novel approach was developed to enhance the remediation capacity of pectin (with a low degree of methylation) by crosslinking it with different agents, namely Ca, Eu, or a combination of the two. Our results showed that Ca, Eu, and their combination induce the gelation of pectin, resulting in a reticulated pectin structure. The type of crosslinking agent used results in significant structural differences that affect the adsorption capacity. The dual-crosslinked pectin film with Ca and Eu atoms had in an intermediate network with both crystalline and non-crystalline regions, exposing more carboxylate anions (COO^- groups) and enabling pectin to simultaneously adsorb heavy metals and pharmaceutical products.

The adsorbent developed in the present work had heavy metal and TC removal efficiencies (in simultaneous experiments) of 94.5% and 93.6%, respectively, at a pH of 7. The removal efficiencies will be optimized further in future work by analyzing the effect of pH, adsorbent dosage, and degree of crosslinking. In addition, more work is necessary to implement this adsorbent in water treatment plants. This includes evaluating the volume of treated water and time for decontamination, which will be part of our future work.

Overall, our novel approach of crosslinking pectin with different agents has the potential to remarkably enhance its remediation capacity for the simultaneous removal of various contaminants, thereby providing an effective and sustainable solution for water pollution management.

Declaration of Competing Interest

The authors declare the following financial interests/personal relationships which may be considered as potential competing interests: [Silvina Cerveny reports financial support was provided by Consejo Superior de Investigaciones Científicas. Silvina Cerveny has patent COMPOSITION FOR REMOVING PHARMACEUTICALS AND HEAVY METALS pending to 22383090.].

Data availability

Data will be made available on request.

Acknowledgments

This work was supported by the Ministerio de Ciencia, Innovación y Universidades code PID2019-104650GB-C21 (MCIN/AEI/10.13039/501100011033), CSIC (I-COOP2020 COOPB20502), and IT1566-22 (Basque Government). We thank Yuri Rakovich and Alba Maria Jumbo Nogales for their assistance during the fluorescence measurements.

Appendix A. Supplementary data

Supplementary data to this article can be found online at https://doi.org/10.1016/j.cej.2023.146162.

References

[1] X.X.Q. Han, E. Hua, B.A. Engel, J.J. Guan, J.L. Yin, N. Wu, S.K. Sun, Y.B. Wang, Understanding implications of climate change and socio-economic development for the water-energy-food nexus: a meta-regression analysis, Agric Water Manag 269 (2022) 12, https://doi.org/10.1016/j.agwat.2022.107693.

[2] J.E. Rodriguez-Gutierrez, A. Castillo-Molar, L.F. Fuentes-Cortes, A multi-objective assessment for the water-energy-food nexus for rural distributed energy systems, Sustain. Energy Technol. Assess. 51 (2022) 15, https://doi.org/10.1016/j.seta.2022.101956.

[3] J.L. Wilkinson, A.B.A. Boxall, D.W. Kolpin, K.M.Y. Leung, R.W.S. Lai, C. Galbán-Malagón, A.D. Adell, J. Mondon, M. Metian, R.A. Marchant, A. Bouzas-Monroy, A. Cuni-Sanchez, A. Coors, P. Carriquiriborde, M. Rojo, C. Gordon, M. Cara, M. Moermond, T. Luarte, V. Petrosyan, Y. Perikhanyan, C.S. Mahon, C.J. McGurk, T. Hofmann, T. Kormoker, V. Iniguez, J. Guzman-Otazo, J.L. Tavares, F. Gildasio De Figueiredo, M.T.P. Razzolini, V. Dougnon, G. Gbaguidi, O. Traoré, J.M. Blais, L. E. Kimpe, M. Wong, D. Wong, R. Ntchantcho, J. Pizarro, G.-G. Ying, C.-E. Chen, M. Páez, J. Martínez-Lara, J.-P. Otamonga, J. Poté, S.A. Ifo, P. Wilson, S. Echeverría-Sáenz, N. Udikovic-Kolic, M. Milakovic, D. Fatta-Kassinos, L. Ioannou-Ttofa, V. Belušová, J. Vymazal, M. Cárdenas-Bustamante, B.A. Kassa, J. Garric, A. Chaumot, P. Gibba, I. Kunchulia, S. Seidensticker, G. Lyberatos, H. P. Halldórsson, M. Melling, T. Shashidhar, M. Lamba, A. Nastiti, A. Supriatin, N. Pourang, A. Abedini, O. Abdullah, S.S. Gharbia, F. Pilla, B. Chefetz, T. Topaz, K. M. Yao, B. Aubakirova, R. Beisenova, L. Olaka, J.K. Mulu, P. Chatanga, V. Ntuli, N. T. Blama, S. Sherif, A.Z. Aris, L.J. Looi, M. Niang, S.T. Traore, R. Oldenkamp, O. Ogunbanwo, M. Ashfaq, M. Iqbal, Z. Abdeen, A. O'Dea, J.M. Morales-Saldaña, M. Custodio, H. de la Cruz, I. Navarrete, F. Carvalho, A.B. Gogra, B.M. Koroma, V. Cerkvenik-Flajs, M. Gombač, M. Thwala, K. Choi, H. Kang, J.L.C. Ladu, A. Rico, P. Amerasinghe, A. Sobek, G. Horlitz, A.K. Zenker, A.C. King, J.-J. Jiang, R. Kariuki, M. Tumbo, U. Tezel, T.T. Onay, J.B. Lejju, Y. Vystavna, Y. Vergeles, H. Heinzen, A. Pérez-Parada, D.B. Sims, M. Figy, D. Good, C. Teta, Pharmaceutical pollution of the world's rivers, PNAS 119 (8) (2022), e2113947119, https://doi.org/10.1073/pnas.2113947119.

[4] M. Nasrollahzadeh, M. Sajjadi, S. Iravani, R.S. Varma, Starch, cellulose, pectin, gum, alginate, chitin and chitosan derived (nano)materials for sustainable water treatment: a review, Carbohydr. Polym. 251 (2021), 116986, https://doi.org/10.1016/j.carbpol.2020.116986.

[5] W. Zhang, J. Song, Q. He, H. Wang, W. Lyu, H. Feng, W. Xiong, W. Guo, J. Wu, L. Chen, Novel pectin based composite hydrogel derived from grapefruit peel for enhanced Cu(II) removal, J. Hazard. Mater. 384 (2020), 121445, https://doi.org/10.1016/j.jhazmat.2019.121445.

[6] S. Thakur, J. Chaudhary, V. Kumar, V.K. Thakur, Progress in pectin based hydrogels for water purification: trends and challenges, J. Environ. Manage. 238 (2019) 210–223, https://doi.org/10.1016/j.jenvman.2019.03.002.

[7] J. Martínez-Sabando, F. Coin, J.H. Melillo, S.N. Goyanes, S. Cerveny, A review of pectin-based material for applications in water treatment, Materials (2023).

[8] G.A. Luzio, R.G. Cameron, Demethylation of a model homogalacturonan with the salt-independent pectin methylesterase from citrus: Part II. structure–function analysis, Carbohydr. Polym. 71 (2) (2008) 300–309.

[9] I. Braccini, S. Pérez, Molecular basis of Ca2+-induced gelation in alginates and pectins: the egg-box model revisited, Biomacromolecules 2 (4) (2001) 1089–1096, https://doi.org/10.1021/bm010008g.

[10] G.T. Grant, E.R. Morris, D.A. Rees, P.J.C. Smith, D. Thom, Biological interactions between polysaccharides and divalent cations: the egg-box model, FEBS Lett. 32 (1) (1973) 195–198, https://doi.org/10.1016/0014-5793(73)80770-7.

[11] E.R. Morris, D.A. Powell, M.J. Gidley, D.A. Rees, Conformations and interactions of pectins: I. Polymorphism between gel and solid states of calcium polygalacturonate, J. Mol. Biol. 155 (4) (1982) 507–516, https://doi.org/10.1016/0022-2836(82)90484-3.

[12] I. Ventura, J. Jammal, H. Bianco-Peled, Insights into the nanostructure of low-methoxyl pectin–calcium gels, Carbohydr. Polym. 97 (2) (2013) 650–658, https://doi.org/10.1016/j.carbpol.2013.05.055.

[13] Y. Fang, S. Al-Assaf, G.O. Phillips, K. Nishinari, T. Funami, P.A. Williams, Binding behavior of calcium to polyuronates: comparison of pectin with alginate, Carbohydr. Polym. 72 (2) (2008) 334–341, https://doi.org/10.1016/j.carbpol.2007.08.021.

[14] M. Celus, C. Kyomugasho, A.M. Van Loey, T. Grauwet, M.E. Hendrickx, Influence of pectin structural properties on interactions with divalent cations and its associated functionalities, Compr. Rev. Food Sci. Food Saf. 17 (6) (2018) 1576–1594, https://doi.org/10.1111/1541-4337.12394.
[15] A. Assifaoui, A. Lerbret, H.T.D. Uyen, F. Neiers, O. Chambin, C. Loupiac, F. Cousin, Structural behaviour differences in low methoxy pectin solutions in the presence of divalent cations (Ca2+ and Zn2+): a process driven by the binding mechanism of the cation with the galacturonate unit, Soft Matter 11 (3) (2015) 551–560, https://doi.org/10.1039/C4SM01839G.
[16] M. Kamruzzaman, A.-M. Alam, S.H. Lee, D. Ragupathy, Y.H. Kim, S.-R. Park, S. H. Kim, Spectrofluorimetric study of the interaction between europium(III) and moxifloxacin in micellar solution and its analytical application, Spectrochim. Acta A Mol. Biomol. Spectrosc. 86 (2012) 375–380, https://doi.org/10.1016/j.saa.2011.10.051.
[17] M.S. Attia, A.M. Othman, A.O. Youssef, E. El-Raghi, Excited state interaction between Hydrochlorothiazide and europium ion in PMMA polymer and its application as optical sensor for Hydrochlorothiazide in tablet and serum samples, J. Lumin. 132 (8) (2012) 2049–2053, https://doi.org/10.1016/j.jlumin.2012.03.012.
[18] L. Liu, G. Chen, M.L. Fishman, A single sorbent for tetracycline enrichment and subsequent solid-matrix time-resolved luminescence, Anal. Chim. Acta 528 (2) (2005) 261–268, https://doi.org/10.1016/j.aca.2004.10.053.
[19] C.A. Destefani, L.C. Motta, R.A. Costa, C.J. Macrino, J.F.P. Bassane, J.F.A. Filho, E. M. Silva, S.J. Greco, M.T.W.D. Carneiro, D.C. Endringer, W. Romão, Evaluation of acute toxicity of europium–organic complex applied as a luminescent marker for the visual identification of gunshot residue, Microchem. J. 124 (2016) 195–200, https://doi.org/10.1016/j.microc.2015.08.021.
[20] J. Wang, X. Guo, Adsorption isotherm models: classification, physical meaning, application and solving method, Chemosphere 258 (2020), 127279, https://doi.org/10.1016/j.chemosphere.2020.127279.
[21] J. Wang, X. Guo, Adsorption kinetic models: physical meanings, applications, and solving methods, J. Hazard. Mater. 390 (2020), 122156, https://doi.org/10.1016/j.jhazmat.2020.122156.
[22] Q.-S. Liu, T. Zheng, P. Wang, J.-P. Jiang, N. Li, Adsorption isotherm, kinetic and mechanism studies of some substituted phenols on activated carbon fibers, Chem. Eng. J. 157 (2) (2010) 348–356, https://doi.org/10.1016/j.cej.2009.11.013.
[23] K.Y. Foo, B.H. Hameed, Insights into the modeling of adsorption isotherm systems, Chem. Eng. J. 156 (1) (2010) 2–10, https://doi.org/10.1016/j.cej.2009.09.013.
[24] J.P. Vareda, On validity, physical meaning, mechanism insights and regression of adsorption kinetic models, J. Mol. Liq. 376 (2023), 121416, https://doi.org/10.1016/j.molliq.2023.121416.
[25] N. Sivagangi Reddy, K. Madhusudana Rao, T.J. Sudha Vani, K.S.V. Krishna Rao, Y. I. Lee, Pectin/poly(acrylamide- co -acrylamidoglycolic acid) pH sensitive semi-IPN hydrogels: selective removal of Cu 2+ and Ni 2+ , modeling, and kinetic studies, Desalin. Water Treat. 57 (14) (2016) 6503–6514.
[26] M.N. Huda, W. Li, M. Dai, L. Lin, Kinetic Study on Mercury Sorption from Fuel Gas, Energy Fuel 31 (2) (2017) 1820–1824, https://doi.org/10.1021/acs.energyfuels.6b02784.
[27] M.M. Bhuyan, H. Okabe, Y. Hidaka, K. Hara, Pectin-[(3-acrylamidopropyl) trimethylammonium chloride-co-acrylic acid] hydrogel prepared by gamma radiation and selectively silver (Ag) metal adsorption, J. Appl. Polym. Sci. 135 (8) (2018) 45906, https://doi.org/10.1002/app.45906.
[28] A. Assifaoui, C. Loupiac, O. Chambin, P. Cayot, Structure of calcium and zinc pectinate films investigated by FTIR spectroscopy, Carbohydr. Res. 345 (7) (2010) 929–933, https://doi.org/10.1016/j.carres.2010.02.015.
[29] A. Balaria, S. Schiewer, Assessment of biosorption mechanism for Pb binding by citrus pectin, Sep. Purif. Technol. 63 (3) (2008) 577–581, https://doi.org/10.1016/j.seppur.2008.06.023.
[30] Z. Veisi, N.D. Gallant, N.A. Alcantar, R.G. Toomey, Responsive coatings from naturally occurring pectin polysaccharides, Colloids Surfaces B: Biointerfaces 176 (2019) 387–393, https://doi.org/10.1016/j.colsurfb.2018.12.060.
[31] N.S. Murthy, H. Minor, General procedure for evaluating amorphous scattering and crystallinity from X-ray diffraction scans of semicrystalline polymers, Polymer 31 (6) (1990) 996–1002, https://doi.org/10.1016/0032-3861(90)90243-R.
[32] L. Li, Y. Fang, R. Vreeker, I. Appelqvist, E. Mendes, Reexamining the egg-box model in calcium−alginate gels with x-ray diffraction, Biomacromolecules 8 (2) (2007) 464–468, https://doi.org/10.1021/bm060550a.
[33] M.D. Walkinshaw, S. Arnott, Conformations and interactions of pectins: II. Models for junction zones in pectinic acid and calcium pectate gels, J. Mol. Biol. 153 (4) (1981) 1075–1085, https://doi.org/10.1016/0022-2836(81)90468-X.
[34] W. Mackie, Conformations of crystalline alginic acids and their salts, Proceed. Biochem. Soc. 125 (4) (1971) 89.
[35] D.A. Powell, E.R. Morris, M.J. Gidley, D.A. Rees, Conformations and interactions of pectins: II. Influence of residue sequence on chain association in calcium pectate gels, J. Mol. Biol. 155 (4) (1982) 517–531, https://doi.org/10.1016/0022-2836(82)90485-5.
[36] D.-Q. Li, J. Li, H.-L. Dong, X. Li, J.-Q. Zhang, S. Ramaswamy, F. Xu, Pectin in biomedical and drug delivery applications: a review, Int. J. Biol. Macromol. 185 (2021) 49–65, https://doi.org/10.1016/j.ijbiomac.2021.06.088.
[37] X.J. Liu, Y.Z. Li, Y.X. Ci, Time-resolved fluorescence studies of the interaction of the Eu3+ complexes of tetracycline analogues with DNA, Anal. Chim. Acta 345 (1–3) (1997) 213–217, https://doi.org/10.1016/s0003-2670(97)00084-6.
[38] F.R.d.O. Silva, R.E. Samad, L. Gomes, L.C. Courrol, Enhancement of europium emission band of europium tetracycline complex in the presence of cholesterol, J. Fluoresc. 18 (1) (2008) 169–174.
[39] M. Jezowska-Bojczuk, L. Lambs, H. Kozlowski, G. Berthon, Metal ion-tetracycline interactions in biological fluids. 10. Structural investigations on copper(II) complexes of tetracycline, oxytetracycline, chlortetracycline, 4-(dedimethylamino) tetracycline, and 6-desoxy-6-demethyltetracycline and discussion of their binding modes, Inorg. Chem. 32 (4) (1993) 428–437, https://doi.org/10.1021/ic00056a015.
[40] L.M. Hirschy, E.V. Dose, J.D. Winefordner, Lanthanide-sensitized luminescence for the detection of tetracyclines, Anal. Chim. Acta 147 (1983) 311–316, https://doi.org/10.1016/0003-2670(83)80097-X.
[41] S. Gago, J.A. Fernandes, J.P. Rainho, R.A. Sá Ferreira, M. Pillinger, A.A. Valente, T. M. Santos, L.D. Carlos, P.J.A. Ribeiro-Claro, I.S. Gonçalves, H. Luminescent, Tris (β-diketonate)europium(III), complexes immobilized in a functionalized mesoporous silica, Chem. Mater. 17 (20) (2005) 5077–5084, https://doi.org/10.1021/cm0514490.
[42] J. Georges, S. Ghazarian, Study of europium-sensitized fluorescence of tetracycline in a micellar solution of Triton X-100 by fluorescence and thermal lens spectrometry, Anal. Chim. Acta 276 (2) (1993) 401–409, https://doi.org/10.1016/0003-2670(93)80411-D.
[43] M. Zhai, B. Fu, Y. Zhai, W. Wang, A. Maroney, A.A. Keller, H. Wang, J.-M. Chovelon, Simultaneous removal of pharmaceuticals and heavy metals from aqueous phase via adsorptive strategy: a critical review, Water Res. 236 (2023), 119924, https://doi.org/10.1016/j.watres.2023.119924.
[44] J. Yan, X. Zuo, S. Yang, R. Chen, T. Cai, D. Ding, Evaluation of potassium ferrate activated biochar for the simultaneous adsorption of copper and sulfadiazine: competitive versus synergistic, J. Hazard. Mater. 424 (2022), 127435, https://doi.org/10.1016/j.jhazmat.2021.127435.
[45] M.H. Kafshgari, M. Mansouri, M. Khorram, S.R. Kashani, Kinetic modeling: a predictive tool for the adsorption of zinc ions onto calcium alginate beads, Int. J. Ind. Chem. 4 (1) (2013) 5, https://doi.org/10.1186/2228-5547-4-5.
[46] K. Rouibah, H. Ferkous, A. Delimi, T. Himeur, M. Benamira, M. Zighed, A. S. Darwish, T. Lemaoui, K.K. Yadav, J.K. Bhutto, A. Ahmad, S. Chaiprapat, Y. Benguerba, Biosorption of zinc (II) from synthetic wastewater by using Inula Viscosa leaves as a low-cost biosorbent: Experimental and molecular modeling studies, J. Environ. Manage. 326 (2023), 116742, https://doi.org/10.1016/j.jenvman.2022.116742.
[47] D. Hu, L. Wang, Adsorption of ciprofloxacin from aqueous solutions onto cationic and anionic flax noil cellulose, Desalin. Water Treat. 57 (58) (2016) 28436–28449, https://doi.org/10.1080/19443994.2016.1183232.
[48] X. Zhang, X. Lin, H. Ding, Y. He, H. Yang, Y. Chen, X. Chen, X. Luo, Novel alginate particles decorated with nickel for enhancing ciprofloxacin removal: Characterization and mechanism analysis, Ecotoxicol. Environ. Saf. 169 (2019) 392–401, https://doi.org/10.1016/j.ecoenv.2018.11.044.
[49] X. Zhang, X. Lin, Y. He, Y. Chen, X. Luo, R. Shang, Study on adsorption of tetracycline by Cu-immobilized alginate adsorbent from water environment, Int. J. Biol. Macromol. 124 (2019) 418–428, https://doi.org/10.1016/j.ijbiomac.2018.11.218.
[50] L. Lu, M. Liu, Y. Chen, Y. Luo, Effective removal of tetracycline antibiotics from wastewater using practically applicable iron(III)-loaded cellulose nanofibres, R. Soc. Open Sci. 8 (8) (2021), 210336, https://doi.org/10.1098/rsos.210336.